Scattering from extended targets in range-dependent fluctuating ocean-waveguides with clutter from theory and experiments

Srinivasan Jagannathan
Massachusetts Institute of Technology, 77 Massachusetts Avenue, Cambridge, Massachusetts 02139

Elizabeth T. Küsel and Purnima Ratilal
Department of Electrical and Computer Engineering, Northeastern University, Boston, Massachusetts 02115

Nicholas C. Makris[a)]
Massachusetts Institute of Technology, 77 Massachusetts Avenue, Cambridge, Massachusetts 02139

(Received 22 August 2011; revised 14 May 2012; accepted 17 May 2012)

Bistatic, long-range measurements of acoustic scattered returns from vertically extended, air-filled tubular targets were made during three distinct field experiments in fluctuating continental shelf waveguides. It is shown that Sonar Equation estimates of mean target-scattered intensity lead to large errors, differing by an order of magnitude from both the measurements and waveguide scattering theory. The use of the Ingenito scattering model is also shown to lead to significant errors in estimating mean target-scattered intensity in the field experiments because they were conducted in range-dependent ocean environments with large variations in sound speed structure over the depth of the targets, scenarios that violate basic assumptions of the Ingenito model. Green's theorem based full-field modeling that describes scattering from vertically extended tubular targets in range-dependent ocean waveguides by taking into account nonuniform sound speed structure over the target's depth extent is shown to accurately describe the statistics of the targets' scattered field in all three field experiments. Returns from the man-made targets are also shown to have a very different spectral dependence from the natural target-like clutter of the dominant fish schools observed, suggesting that judicious multi-frequency sensing may often provide a useful means of distinguishing fish from man-made targets. © *2012 Acoustical Society of America*.
[http://dx.doi.org/10.1121/1.4726073]

PACS number(s): 43.30.Gv, 43.20.Fn [KML] Pages: 680–693

I. INTRODUCTION

Vertically extended air-filled tubular targets[1] are often used at sea in long range acoustic experiments[2] as a ground truth reference to check and calibrate full-field waveguide scattering models, target strength estimates from other distant objects, and an aid in navigation and charting,[2] due to their high target strength. When modeling scattering from such extended targets in range- and depth-dependent fluctuating waveguides, it is not possible to make simplifying assumptions such as the factorability of propagation and scattering[3] assumed in the Sonar Equation[4] or the iso-sound speed assumption[3] of the Ingenito scattering model.[5] In this paper, Green's theorem-based full-field modeling that describes scattering from vertically extended tubular targets is shown to accurately describe scattered field statistics measured during three distinct field experiments. Key elements of the model are its ability to accurately treat the effects of potentially nonuniform sound speed structure over the target's depth extent, range dependence, and oceanographic fluctuations that lead to transmission scintillation, all of which are often encountered in natural ocean waveguides.

Bistatic, long-range, low-frequency measurements of acoustic returns from vertically extended air-filled cylindrically shaped targets were made during three field experiments sponsored by the Office of Naval Research (ONR). Two of these experiments were carried out in the New Jersey continental shelf region during May–June 2001 (Ref. 2) and 2003 (Refs. 6 and 7) (NJ2001 and NJ2003), and the third experiment was carried out in Georges Bank during Sep–Oct 2006 (Refs. 8 and 9) (GOM2006). During all three experiments, Ocean Acoustic Waveguide Remote Sensing (OAWRS) systems[7,9] were used to image passive acoustic targets, which were vertically suspended from the seafloor using floats and anchors so that they occupied specified water depths. These man-made targets were manufactured by BBN Technologies[1] (Cambridge, MA) and consisted of 30-m long and 7-cm diameter air-filled tubular hoses made of gum rubber. The acoustic returns from these targets were measured across multiple frequency bands ranging from 415 to 1325 Hz.

Besides man-made targets, target-like clutter were also imaged during all three experiments. Atlantic herring schools were found to be the dominant cause of such target-like clutter imaged during the NJ2003 and GOM2006 experiments.[7,9] Even when echo returns from the dominant fish species encountered and the tubular man-made targets have similar spatial characteristics and scattered intensity levels, their spectral dependencies are shown to be very different, making them robustly distinguishable by multi-frequency measurements.

The target-scattered data from all three field experiments are also used to assess the performance of the Sonar

[a)]Author to whom correspondence should be addressed. Electronic mail: makris@mit.edu

 0001-4966/2012/132(2)/680/14/$30.00

Equation model,[4] the Ingenito scattering model,[5] and the Vertically Extended Cylindrical Target Waveguide Scattering (VETWS) model.[10] Mean intensities of returns scattered by the man-made targets estimated with the VETWS model are shown to reliably match measured values to within the 3 dB data standard deviation in all three experiments. Sonar Equation estimates of mean scattered intensity from the targets lead to large errors, however, typically differing by 10 dB from both measurements and waveguide scattering theory. Similarly large errors are also found in estimates made with the Ingenito scattering model.

Some major discrepancies between measured scattered returns and estimates obtained using both the Sonar Equation and the Ingenito scattering model are due to the inadequacy of some basic assumptions of these models for highly directional targets in non-iso sound speed layers. The Sonar Equation model, for example, has been shown by theory and simulation to be generally valid in an ocean waveguide only for objects that have an omnidirectional or monopole scatter function over the incident and scattered directions at the target and to typically be a poor approximation for objects with large directionality over this range.[3] In an ocean waveguide, propagation, to and from a target, is convolved with scattering from the target and can only be factored as in the Sonar Equation given this omnidirectional or monopole condition. The monopole approximation is valid for many compact gas-filled targets, small compared to the acoustic wavelength. The air-filled cylindrical targets considered here are large compared to the acoustic wavelength and are highly directional, so the discrepancy found experimentally between their target returns and those estimated by the Sonar Equation is consistent with theory and past simulations.[3]

The Ingenito scattering model accounts for the coupling of incident and scattered modes[5] through a far-field scattering approximation but only applies to objects contained within an iso-sound speed depth layer in a range-independent ocean waveguide. In all three experiments considered here in typical continental shelf environments, the sound speed variations over the depth of the vertically extended targets (5–10 m/s) are significant because they lead to ray angle changes on the order of both the seafloor critical angle and the target's effective beamwidth defined by the wavelength to target length ratio. Sound speed variations over the depth of the target then not only lead to significant changes in the interference structure of the scattered field but also changes in the amount of acoustic energy in the trapped waveguide modes that are most crucial to long range propagation. This is similar to effects observed from target directionality variations in an ocean waveguide.[3] Sound speed variations over the target depth led to the most significant violations of the Ingenito model assumptions in the NJ2001 and NJ2003 environments that were nearly range independent, while both vertical sound speed variations as well as significant range dependence led to major violations of Ingenito model assumptions in the GOM2006 environment.

The VETWS model can be applied to both pressure-release and penetrable cylindrical targets that are vertically extended in an ocean waveguide.[10] Here we use the pressure-release VETWS model, which is suitable for modeling scattering from the air-filled cylindrical targets that were used in all the three field experiments considered in this paper. In this model, the scattered field in the vicinity of the target is expressed in terms of Hankel functions, the coefficients of which are determined by matching appropriate boundary conditions on the surface of the target. By allowing the coefficients to vary with the depth of the target, the effects of incident field refraction are taken into account. While Ref. 10 provides an approximate numerical recipe to determine these coefficients, an alternative approach is used in this paper by explicitly deriving their analytical expressions.

The arrival structure and dispersion of scattered acoustic returns from man-made targets is quantified by implementing the matched-filter.[11–13] By studying the effects of waveguide dispersion on the arrival structure of scattered returns, it is shown that the targets may appear in sonar imagery either as sharp, well localized returns with high signal-to-noise ratio (SNR) (>10 dB) or as dispersed returns with low SNR. It is then important to have accurate knowledge of oceanography when trying to model scattering from such targets in continental shelf environments. Fluctuations in oceanography, such as the sound speed structure, are shown to affect the ability to localize the man-made targets in a waveguide. To account for the scintillation in the measured scattered intensity caused by fluctuations of the ocean waveguide, Monte Carlo simulations of the scattered field are computed by implementing all three scattering models, the Sonar Equation, Ingenito, and VETWS in a waveguide randomized by internal waves.

The three experimental scenarios where bi-static measurements of scattering from vertically extended air-filled cylindrical targets were made are described in the next section. In Sec. III, the general characteristics of the target-scattered field from all three experiments, including spectral dependence of scattered returns, are described. Broad-spectrum measurements of the target scattered field are also shown to help distinguish such man-made targets from natural biological clutter such as fish schools that appear to be similar in single frequency long range sonar imagery. In Sec. IV, the theoretical approach and analytical formulation for scattering from the man-made targets are presented. In Sec. V, comparisons are made of the measured statistics of target returns from all three experiments with (1) the Sonar Equation model, (2) the Ingenito scattering model, and (3) the VETWS model. It is shown that both the sonar equation and the Ingenito scattering models lead to large errors (>5 dB), while the full-field model is shown to be most accurate (errors <3 dB) in describing the measured mean and standard deviation of the target-scattered levels.

II. DESCRIPTION OF FIELD EXPERIMENTS

A. The 2001 experiment of the ONR Geoclutter Program

The ONR-sponsored NJ2001 experiment that took place in the New Jersey continental shelf from April 17 to May 5, 2001, was designed to (1) study spatial and temporal variability of clutter in long-range active sonar, (2) identify dominant sources of clutter and understand their physical mechanisms,

and (3) examine bistatic scattering characteristics of clutter.[2] Figures 1(A) and 1(B) show the bathymetry contours in the New Jersey continental shelf and the geometry of two tracks during the NJ2001 experiment, respectively. The experimental design consisted of a moored vertical source array and a horizontal receiving array that was separately deployed allowing bistatic measurements of echo returns. Broadband Tukey-windowed linear frequency modulated (LFM) pulses 1s in duration and 50 Hz band-width were transmitted at frequencies centered at 375, 415, 750, and 1500 Hz. The study area represents a typical continental shelf environment with a fairly constant bathymetry but highly varied oceanography. Monitoring of the physical oceanography was carried out concurrently with the acoustic sensing experiment. Measurements of water column temperature and salinity were taken regularly using expendable bathythermographs (XBT) and conductivity, temperature, depth (CTD) sensors. The measured water column sound speed profiles are used as inputs in the modeling of the scattered returns from air-filled cylindrical targets.

B. The 2003 experiment of the ONR Geoclutter Program

The New Jersey continental shelf region was studied again during the NJ2003 experiment, which was designed to establish actual mechanisms of clutter and reverberation[14] including scattering from large fish shoals[6,7] as well as calibrated air-filled targets. The geometry of two tracks during the experiment is shown in Fig. 1(C). During the experiment, 1-s long LFM waveforms of 50-Hz bandwidth centered at 415, 950, and 1325 Hz were transmitted, enabling multi-spectral analysis of echo returns. Monitoring of the physical oceanography occurred concurrently with the acoustic sensing experiment. Here XBT/CTD-based measurements of water column sound speed profiles are used to generate multiple realizations of a fluctuating ocean environment for Monte Carlo modeling of the scattered returns from the air-filled cylindrical targets.

C. The 2006 experiment of the National Oceanographic Partnership Program (NOPP)

The NOPP-sponsored GOM2006 experiment that took place in the Gulf of Maine from Sep. 19 to Oct. 6, 2006, was designed to study the scattering characteristics and behavior[8] of Atlantic herring (*Clupea harengus*) through wide-area images of instantaneous scattered acoustic intensity levels.[9] Figure 2 shows the geometry of the experiment and bathymetry contours near Georges Bank, Gulf of Maine. The experimental design consisted of a moored vertical array and a horizontal receiving array that were separately deployed to allow bistatic measurements of echo returns. Broadband Tukey-windowed LFM pulses 1s in duration and 50 Hz bandwidth were transmitted at frequencies centered at 415,

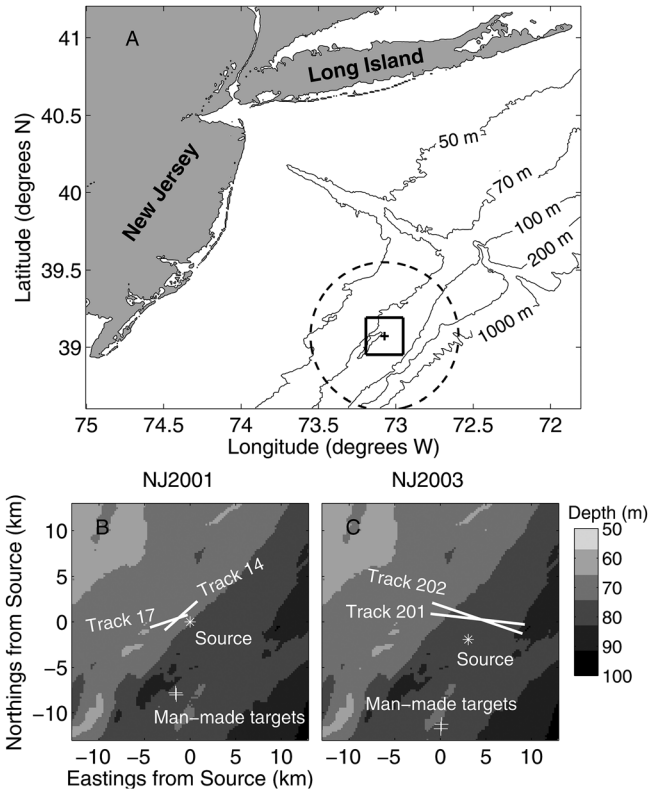

FIG. 1. (A) Location of the NJ2001 and the NJ2003 experiments off the coast of New Jersey. Black dashed circle shows 60-km diameter areal imaging coverage in 40 s. (B) and (C) Geometry of the experiments showing the location of the moored source, the targets, and two receiver tracks in each experiment from which measured target-scattered received levels are used for comparisons with models. The zoom area is shown as a black box in (A). The grayscale shows the relatively flat bathymetry in the region.

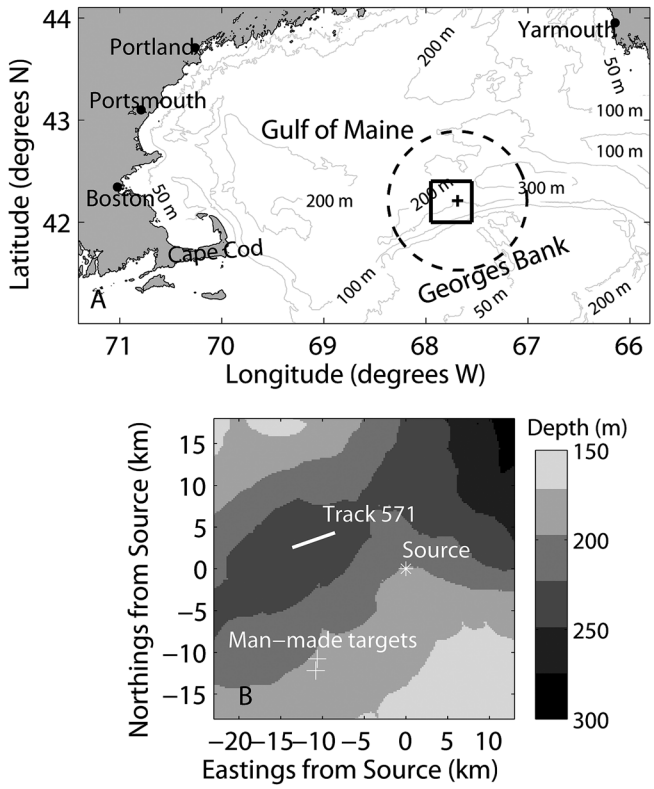

FIG. 2. (A) Location of the GOM2006 experiment in the Gulf of Maine. Bathymetric contours are marked with grey lines. Black dashed circle shows 100-km areal imaging coverage in 75 s. (B) Geometry of the experiment showing the location of the moored source, the targets, and the receiver track from which measured target-scattered received levels are used for comparisons with models. The zoom area is shown as a black box in the left figure. The grayscale shows the highly variable bathymetry in the region.

735, 950, and 1125 Hz. The study area represents a complex continental shelf environment with highly variable bathymetry and oceanography. Concurrent measurements of water column temperature and salinity yielded a total of 186 water column sound speed profiles (SSPs) from the Georges Bank region,[9] and the SSPs are used to generate fluctuating ocean realizations for Monte Carlo modeling of scattered returns from the air-filled cylindrical targets.

III. DISTINGUISHING FISH FROM VERTICALLY EXTENDED TUBULAR MAN-MADE TARGETS USING MULTI-FREQUENCY MEASUREMENTS

Air-filled cylindrical targets were deployed in all three experiments, the NJ2001, NJ2003, and GOM2006, to (1) aid accurate charting of scattered returns onto a geographic grid[2,7,9] and (2) calibrate the data. Across these three experiments, a wide variety of scenarios with different source-target-receiver configurations in highly fluctuating ocean waveguides with varied bathymetry were explored.

In both the NJ2001 and NJ2003 experiments, the centers of the source and the receiver were located at depths of about 32 and 30 m, respectively, in a water-column depth of roughly 70 m. Five targets, centered at water depths of about 44 m, were deployed during each of these two experiments in water-column depths of roughly 80 m. In this paper, one target from each experiment [the southernmost target in Figs. 1(B) and 1(C)] is selected for data-model comparisons based on (1) the target's clear visibility in the sonar image (i.e., received acoustic intensity more than an order of magnitude above background reverberation levels, or SNR $\geq$ 10 dB) and (2) spatial isolation from other clutter features to ensure that the target-scattered returns are not contaminated with other clutter returns. These targets were typically 10 km away from both the source and the receiver as seen in Figs. 1(B) and 1(C). Figure 3 shows the clear appearance of the targets in sonar imagery during both NJ2001 and NJ2003 experiments, respectively. The returns from man-made targets are at least an order of magnitude larger than returns from the background (SNR $\geq$ 10 dB). The targets appear elongated in OAWRS imagery because the range resolution is much finer than the azimuth resolution of the OAWRS receiving array. The range resolution for the 50-Hz bandwidth source waveform used in all three experiments is $\approx$15 m.[6] The azimuthal resolution is range dependent and is given by $R\delta\theta$, where R is the distance to the center of the receiving array and $\delta\theta$ is the angular resolution of the array at broadside given by $\delta\theta = \lambda/L_a$, where λ is the acoustic wavelength and L_a is the aperture length.

During the GOM2006 experiment, the source and receiver were located at depths of about 60 and 105 m, respectively, in water-column depths ranging from 180 to 250 m. On Oct. 2, 2006, two air-filled cylindrical targets were deployed at selected locations shown in Fig. 2. The targets were centered at depths of 140 and 180 m in a water-column depth of 200 m, and their distances from the source array were approximately 16 and 15 km, respectively. During the experiment, the 180-m deep target was often not clearly visible in OAWRS images, possibly because of target deflation due to the large hydrostatic pressure at such depths. In this paper, we consider the measurements of scattered intensity across different frequencies from the 140-m deep target when SNR $\geq$ 10 dB.

In all three experiments, the targets appeared as either sharp, well-localized returns [Figs. 4(D)–4(F)] or as weak, dispersed returns [Figs. 4(G)–4(I)]. Such changes in target-scattered field and arrival structure of target-scattered returns are caused by fluctuations in oceanography as we show in Sec. V and in Appendix B. The targets are well-localized when most of the scattered acoustic energy is concentrated in the first few waveguide modes that combine constructively to form a sharp return with high SNR (Appendix B), such as the ones shown in Fig. 3. When the scattered acoustic energy is distributed across more waveguide modes, the later arrival of the higher order modes results in poorly localized, weak returns from the target (Appendix B). The examples shown in

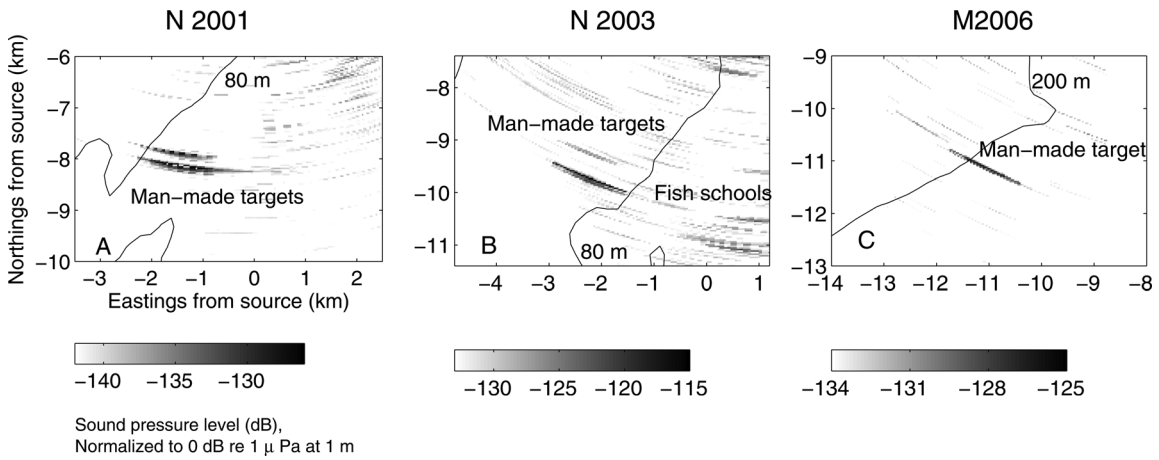

FIG. 3. Discrete, consistent and strong acoustic returns from man-made targets were recorded during (A) NJ2001, (B) NJ2003, and (C) GOM2006. Examples of Ocean Acoustic Waveguide Remote Sensing (OAWRS) sound pressure-level (SPL) image, zoomed around the region of targets, normalized to 0 dB source-level, obtained on (A) May 1, 2001 at 10:58:15 GMT (Ref. 2), (B) May 9, 2003 at 21:19:55 GMT, and (C) October 2, 2006 at 23:10:00 GMT. A linear frequency modulated (LFM) 1-s long pulse with center frequency 415 Hz and bandwidth of 50 Hz was used to form the images. Black lines mark the 80-m isobath in (A) and (B) and the 200-m isobath in (C).

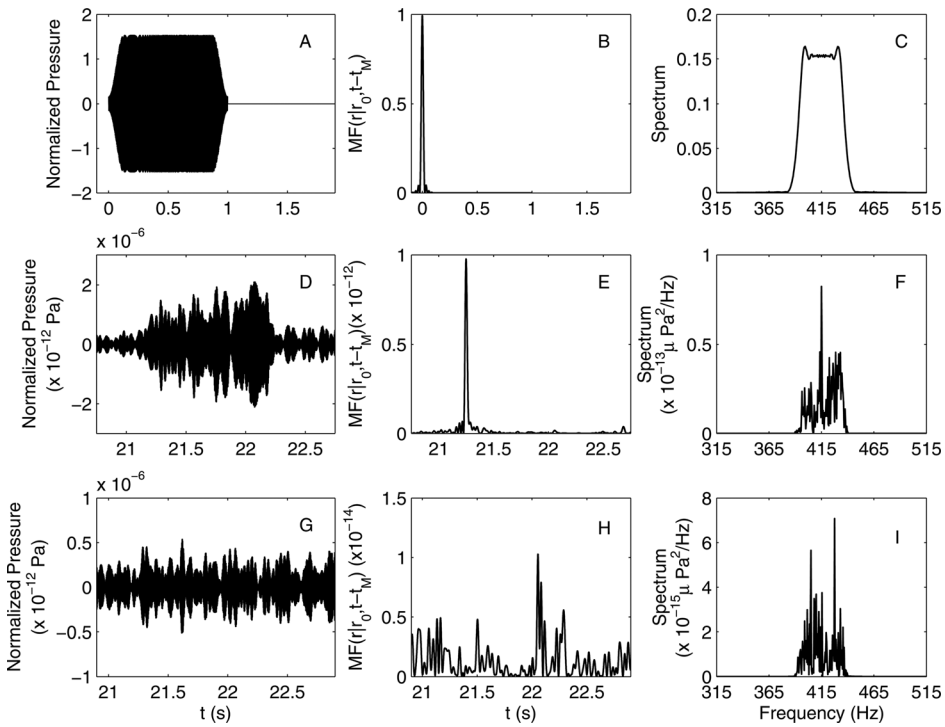

FIG. 4. Examples of typical matched-filter output of man-made target-scattered data recorded during NJ2003. (A)—(C) Transmitted linear frequency modulated (LFM) signal envelope; normalized matched-filter (MF) output of the LFM waveform; and signal spectrum. (D)—(F) Example of envelope of received target-scattered signal before matched filtering recorded on May 9, 2003 at 18:28:15 GMT; the MF output [computed using Eq. (10)] showing sharp, well localized target-return plotted as a function of two-way travel time; and frequency spectrum of the received signal in (D). (G)—(I) Example of envelope of received target-scattered signal before matched-filtering recorded on May 9, 2003 at 18:31:35 GMT (3 min later than D), the MF output [computed using Eq. (10)] showing weak, dispersed, less well-localized target-return plotted as a function of two-way travel time and frequency spectrum of the received signal in (G). Dispersed target returns were observed in roughly 25% of all target returns in NJ2003.

Fig. 4 for the NJ2003 experiment are also representative of target-scattered returns observed during NJ2001 and GOM2006 experiments.

In wide-area OAWRS images, man-made targets often appeared similar to small fish schools. This is illustrated in Fig. 3(B), which shows a wide-area source-level-normalized sound pressure level (SPL) image for a 415 Hz source waveform captured during NJ2003 on May 9. On this day, the presence of fish schools was confirmed by simultaneous *in situ* measurements using a conventional fish finding sonar (CFFS).[6] While returns from both man-made targets and fish schools appear similar at any one particular frequency, the availability of multi-spectral data enables the comparison of acoustic returns across multiple frequencies for spectral trends that can be used to discriminate man-made targets and fish.

The spectral dependence of scattering from fish has been extensively discussed for both the NJ2003 (Ref. 7) and GOM2006 (Ref. 9) experiments. Based on *in situ* CFFS and trawl measurements, Atlantic herring was found to be the major constituent of the fish schools imaged during both the experiments. The target strength of herring in both these experiments has been shown to increase as a function of OAWRS operating frequency.[7,9] Because individual Atlantic herring are found to be acoustically compact (i.e., swimbladder length $\ll$ acoustic wavelength) and to scatter incoherently from other shoaling herring in OAWRS imagery,[7,9,15] a Sonar Equation model was found to accurately describe scattering from herring schools and was used to estimate their frequency-dependent target strength ($\widehat{TS}_{\text{fish}}$). The $\widehat{TS}_{\text{fish}}$ for both the NJ2003 and GOM2006 are shown in Figs. 5(A) and 5(B), respectively.

The Sonar Equation, however, cannot be used to quantify scattering from targets with highly directional scatter functions, such as the air-filled cylindrical targets described in this paper.[3] To compare the frequency response of man-made targets with that of fish, we can still write an expression for a sonar-equation-derived target strength of the man-made target ($\widehat{TS}_{\text{tgt}}$). Such an estimated $\widehat{TS}_{\text{tgt}}$ is the target strength of an equivalent compact scatterer placed at the center of the man-made target, which gives rise to the same received scattered level as that of the man-made target.

The sonar-equation-derived $\widehat{TS}_{\text{tgt}}$ can be estimated from the data by

$$\widehat{TS}_{\text{tgt}} = \text{RL} - \text{SL} + \text{TTL} \tag{1}$$

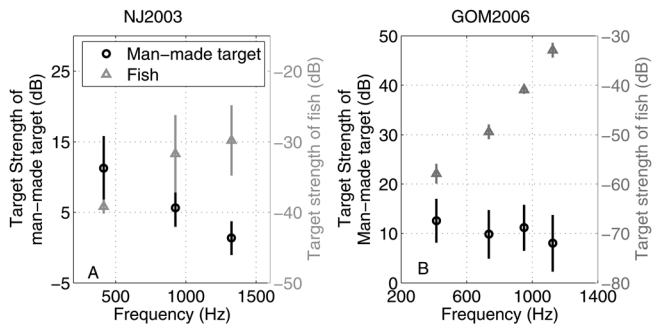

FIG. 5. Sonar Equation-derived targets strengths (TS) of man-made targets vs fish [$\widehat{TS}_{\text{tgt}}$ vs $\widehat{TS}_{\text{fish}}$, Eq. (1)]. Black dashed circles are used to denote mean TS of man-made targets and gray triangles are used to denote TS for fish. (A) $\widehat{TS}_{\text{tgt}}$ vs $\widehat{TS}_{\text{fish}}$ measured on May 9, 2003, during NJ2003. Vertical bars are the standard deviations of the target strength estimates. A total of 85 transmissions from Track 201 were used for estimating $\widehat{TS}_{\text{tgt}}$ at 415 Hz. A total of 90 transmissions from track 202 were used for estimating $\widehat{TS}_{\text{tgt}}$ at 925 and 1325 Hz. To estimate $\widehat{TS}_{\text{fish}}$, data from both May 9 and May 14 were used as described in Ref. 7. (B) $\widehat{TS}_{\text{tgttgt}}$ vs $\widehat{TS}_{\text{fish}}$ measured on Oct. 2, 2006, during GOM2006. A total of 20 transmissions from Track 571 were used for estimating $\widehat{TS}_{\text{tgt}}$ at each frequency shown. To estimate $\widehat{TS}_{\text{fish}}$, data from Oct 2. was used as described in Ref. 9.

where RL is the measured (received) sound pressure level, SL is the known source level, and TTL is the two-way transmission loss averaged over the depth of the target. Transmission loss is computed using the parabolic equation based Range-Dependent Acoustic Model (RAM).[16] The mean and standard deviation of $\widehat{TS}_{\text{tgt}}$, shown in Fig. 5, are computed using several independent TS estimates across different frequencies. For comparison, the mean and standard deviation of the TS of fish ($\widehat{TS}_{\text{fish}}$) are also shown in the same figure.

The TS for fish increases as a function of frequency as can be seen in Fig. 5. This is because the incident acoustic frequencies span the lower half of the resonance peak, where there is a sharp increase of TS for the fish imaged in both the New Jersey continental shelf during NJ2003 and the Gulf of Maine during GOM2006.[7,9] In contrast, the TS of cylindrical targets are observed to follow the opposite trend as a function of frequency. This is because the expected resonance frequency for the extended targets is much lower (about 40–50 Hz)[17] than those for the fish. This difference in frequency response can be used to discern these fish from vertically extended air-filled cylindrical man-made targets.

IV. THEORETICAL FORMULATION

A. Problem geometry

A target-centered cylindrical coordinate system is used (Fig. 6), where $\mathbf{r_t} = (a, \phi_t, z_t)$ is any point on the target's cylindrical surface with $0 \le \phi_t \le 2\pi$ and $-L/2 \le z_t \le L/2$. The total target length is L and the cylinder radius is a. The source is located at $\mathbf{r_0} = (\rho_0, \phi_0, z_0)$ and the receiver at $\mathbf{r} = (\rho, \phi, z)$. The bathymetry and oceanography are modeled as range dependent.

B. Theory

A Greens' Theorem approach[10] is used to calculate the scattered returns from vertically extended cylindrical targets in range-dependent ocean waveguides. The scattered pressure per Hertz at a particular frequency f at the receiver location is expressed as

$$P_{\text{scat}}(\mathbf{r}|\mathbf{r}_0,f) = -\oint_{S_t} [P(\mathbf{r_t}|\mathbf{r}_0,f)\nabla_t G(\mathbf{r}|\mathbf{r_t},f) - \nabla_t P(\mathbf{r_t}|\mathbf{r}_0,f) G(\mathbf{r}|\mathbf{r_t},f)] \cdot \mathbf{n_t}\, dS_t, \quad (2)$$

where $P(\mathbf{r_t}|\mathbf{r_0}, f)$ is the total acoustic pressure per Hertz on target's surface, which is expressed as the sum of incident and scattered waves, $G(\mathbf{r}|\mathbf{r_t}, f)$ is the waveguide's Green function from any point on the target to the receiver, S_t is surface of the target, and $\mathbf{n_t}$ is the normal to the target surface.

A pressure-release condition is assumed at the surface of the cylindrical target. The scattered field on the surface of the target can be expressed as a sum of weighted Hankel functions as described in Ref. 10. Hence, the scattered field at the receiver can be expressed as

$$\begin{aligned} P_{\text{scat}}(\mathbf{r}|\mathbf{r}_0,f) = &-\int_{z_t=-L/2}^{z_t=+L/2}\int_{\phi_t=0}^{2\pi} G(\mathbf{r}|\mathbf{r}_t,f) \\ &\times \frac{\partial P_{\text{inc}}(\mathbf{r_t}|\mathbf{r}_0,f)}{\partial \rho_t}\, a\, dz_t\, d\phi_t \\ &- \int_{z_t=-L/2}^{z_t=+L/2}\int_{\phi_t=0}^{2\pi} G(\mathbf{r}|\mathbf{r}_t,f)\sum_{n=0}^{\infty} A_n(z_t|\mathbf{r}_0,f) \\ &\times \cos(n\phi_t)\left[-k\mathrm{H}_{n+1}^{(1)}(ka) + \frac{n}{a}\mathrm{H}_n^{(1)}(ka)\right] \\ &\times a\, dz_t\, d\phi_t, \end{aligned} \quad (3)$$

where $P_{\text{inc}}(\mathbf{r_t}|\mathbf{r_0}, f)$ is the incident pressure on the target, $A_n(z_t|\mathbf{r_0}, f)$ are depth-dependent coefficients, $\mathrm{H}_n^{(1)}$ is the Hankel function of the first kind and nth order, and $k = 2\pi f/c$ is the wavenumber. The depth and azimuthal dependence of the scatter function are separable due to the cylindrical shape of the targets. Typically this is not possible for an arbitrary-shaped object that is large compared to the acoustic wavelength, in an ocean waveguide.

The first integral in Eq. (3) is evaluated numerically using an acoustic propagation model, such as RAM.[16] To evaluate the second integral, the coefficients A_n must be determined. While Ref. 10 provides an approximate numerical recipe to determine these coefficients, here analytical expressions are derived in Appendix A that are then used in the scattering model.

Besides the VETWS, the Ingenito scattering model and the Sonar Equation model are also implemented to compute scattered returns from the cylindrical targets. The Ingenito scattering model[5,18] was developed to describe far field

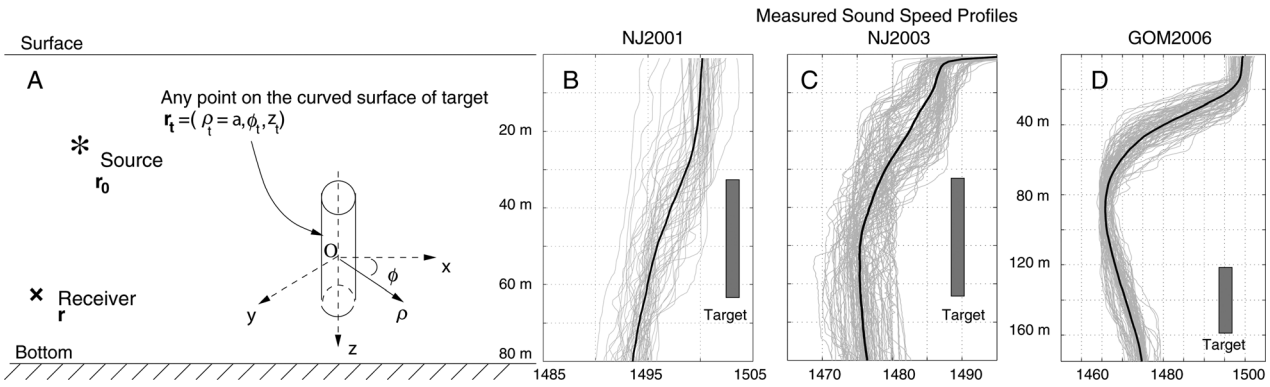

FIG. 6. Geometry (not to scale) showing target-centered cylindrical coordinate system used in the Vertically Extended Cylindrical Target Waveguide Scattering (VETWS) model. The cylinder has length L and radius a. The non-iso sound speed structure over the depth of the man-made extended target, measured during NJ2001, NJ2003 and GOM2006 (gray lines) and their means (black lines) are shown to the right.

scattering from an object within an iso-velocity layer in a range-independent stratified medium. In this model, the scattered field is expressed in terms of up- and down-going incident plane waves coupled with up- and down-going scattered plane waves via the plane wave scatter function of the object [Eq. (51) in Ref. 5 and Eq. (1B) in Ref. 18]. The main difference between Eq. (51) in Ref. 5 and Eq. (1B) in Ref. 18 is the convention used to represent the direction of the incident wave; the former uses *the direction the incident wave comes from* and the latter uses *the direction the incident wave goes to*.[18] Here we use Eq. (1B) from Ref. 18, which is the more standard approach.

The Ingenito scattering model is derived from Green's Theorem [Eq. (8) in Ref. 5, Eq. (A1) in Ref. 18 and Eq. (2)]. For a pressure-release target, the first term in Eq. (2) is zero, and the waveguide Green's function in the second term is expressed as a normal mode sum [Eq. (10) in Ref. 5]. The target is then assumed to be in an iso-velocity layer so that the incident and the scattered field around the target can be expressed as a sum of *plane waves* [Eq. (12) in Ref. 5]. The target is assumed to be in the far field of the source and the receiver,[19] i.e., range $\gg L_s^2/\lambda$, where L_s is the length of the source array and λ is the acoustic wavelength. The local scattered field around the object is approximated as the scattered field in free space [Eq. (C9) in Ref. 5]; this leads to an analytic far field expression for the scattered field when multiple scattering between the waveguide boundaries and the object can be neglected.[18–20] The Ingenito model is restricted to range-independent waveguides because its fundamental formulation is in terms of range-independent normal mode based Green functions.

The scattered field at a receiver located at $\mathbf{r}$ given a source at $\mathbf{r_0}$, using the Ingenito formulation [Eq. (1B) in Ref. 18] is given by

$$\begin{aligned}\Phi_s(\mathbf{r}|\mathbf{r}_0) = \sum_{m,n} \frac{4\pi}{k} [&C_m(\mathbf{r})C_n(\mathbf{r}_0)S(\pi-\alpha_m,\phi;\alpha_n,\phi_0+\pi)\\ &- D_m(\mathbf{r})C_n(\mathbf{r}_0)S(\alpha_m,\phi;\alpha_n,\phi_0+\pi)\\ &- C_m(\mathbf{r})D_n(\mathbf{r}_0)S(\pi-\alpha_m,\phi;\pi-\alpha_n,\phi_0+\pi)\\ &+ D_m(\mathbf{r})D_n(\mathbf{r}_0)S(\alpha_m,\phi;\pi-\alpha_n,\phi_0+\pi)] \quad (4)\end{aligned}$$

where the C_n and D_n are down-going and up-going mode amplitudes of the incident field and C_m and D_m are the up-going and down-going mode amplitudes of the scattered field, respectively,[21] α_n is the elevation angle of the nth mode, ϕ is the azimuthal angle of the receiver, and ϕ_0 is the azimuthal angle of the source. The angle-dependent plane wave scatter function S has been derived in its generalized form using Greens Theorem in Eq. (A7) of Ref. 18 as well as in Ref. 22 for various canonical shapes.

In contrast, while VETWS is also derived directly from Green's theorem, it exploits the cylindrical nature of the target; this leads to an exact expression for the single scattered field in Eq. (3) for arbitrary sound speed variations over the target's depth. For a long and thin, vertically oriented cylindrical target in a waveguide, this is an excellent approximation because multiple scattering between the cylinder and waveguide boundaries can be neglected. Because it employs the PE-based Green functions, the VETWS model is range dependent.

Key differences between the Ingenito and the VETWS models for cylindrical object scattering in ocean waveguides have been described in Ref. 10, where three scenarios were investigated: (1) Pekeris waveguide, which is range independent with constant sound speed over the entire water column, (2) flat bathymetry with a depth-dependent sound speed profile over the layer of the object, and (3) a range-dependent environment with a constant sound speed profile over the object's depth. In the first case, both the Ingenito and the VETWS models yielded identical far field scattered levels (Fig. 2 of Ref. 10) as expected because the two models theoretically converge in this case. In the other two cases where the models do not converge theoretically and the Ingenito approach employs oversimplifications, there was at least 3–5 dB difference between the two approaches; this is consistent with the experimental and numerical findings of this paper.

The Ingenito scattering model has been shown to reduce to the Sonar Equation model in Eq. (32) of Ref. 5 and in Ref. 19 when the target has an effectively omni-directional or monopole scatter function. The scatter function then factors from the double sum in Eq. (4) so that the incident and outgoing summations separate into factors representing the incident and outgoing Green functions with respect to the target. The approximate validity of the sonar equation for scattering in a stratified medium when the object's scatter function is roughly a constant over the horizontal grazing angles of the dominant waveguide modes is demonstrated with simulations in Ref. 3.

V. STATISTICS OF MEASURED AND SIMULATED SCATTERED FIELDS FROM TARGETS

A. Measured returns from passive acoustic targets

For each source transmission from location $\mathbf{r_0}$, the received acoustic pressure, p at time t and at hydrophone location $\mathbf{r}_h$ is first beamformed in azimuth. The beamformed result is given by

$$\Psi(\mathbf{r}|\mathbf{r}_0,t) = \frac{1}{N_h}\sum_{l=-N_h/2}^{N_h/2} p\left(\mathbf{r}_{h,l}|\mathbf{r}_0, t + l\frac{\Delta\sin\theta}{c}\right) \quad (5)$$

where $\mathbf{r}$ is the center of the receiver array, $\mathbf{r}_{h1}$ is the lth hydrophone, N_h is the number of hydrophone elements in the receiver array, Δ is the spacing between array hydrophone elements, c is the sound speed, and θ is the horizontal angle from array broadside to the man-made target. The beamformed output, $\Psi(\mathbf{r}|\mathbf{r_0}, t)$, is Fourier transformed to obtain its complex spectral amplitude $\Phi(\mathbf{r}|\mathbf{r_0}, f)$ for frequency f, following the transform equation

$$\Phi(\mathbf{r}|\mathbf{r}_0,f) = \int_T \Psi(\mathbf{r}|\mathbf{r}_0,t)e^{i2\pi ft}dt, \quad (6)$$

where T is a time window containing the signal. The matched filter[11–13] is then applied and is given by

$$H(f|t_M) = KQ^*(f)e^{i2\pi f t_M} \tag{7}$$

where t_M is the time delay of the matched-filter and K is related to the total energy in the input signal and is given by

$$K = \left(\int |Q(f)|^2 df\right)^{-1/2} \tag{8}$$

and $Q(f)$ is the source spectrum. The time delay corresponds to two-way travel time from the source to the man-made target and back to the receiver. The time-dependent matched-filtered scattered return is then computed by Fourier synthesis as

$$\chi(\mathbf{r}|\mathbf{r}_0, t - t_M) = \int \Phi(\mathbf{r}|\mathbf{r}_0, f)H(f|t_M)e^{-i2\pi f t} df. \tag{9}$$

The maximum matched-filter output is then

$$\mathrm{MF}(\mathbf{r}|\mathbf{r}_0, t_M) = \max_t \left| \int \Phi(\mathbf{r}|\mathbf{r}_0, f)KQ^*(f)e^{-i2\pi f(t-t_M)}\, df \right|^2. \tag{10}$$

For illustration, the source signal characteristics for the NJ2003 experiment at a center frequency of 415 Hz are shown in Figs. 4(A)–4(C). Similar plots for the normalized transmitted signal amplitude [Fig. 4(A)], the corresponding matched filtered signal [Fig. 4(B)], and the signal spectrum [Fig. 4(C)] can also be obtained for the different transmitting frequencies used in all three experiments.

Figure 4(E) shows the MF output of the received signal for a target-receiver separation of 12.45 km, after waveguide propagation and scattering from targets, measured during NJ2003. The matched filter picks the true location of the target, shown as a sharp peak in Fig. 4(E). However, the MF output of the scattered signal from the target is not always sharp but was dispersed roughly 25% of the time in NJ2003 experiment for example as illustrated in Fig. 4(H) in which a clear peak is not observed. This is due to waveguide dispersion, which causes higher order modes to arrive later at the receiver.[13] This effect is quantified by simulating the MF output for different oceanographic conditions in Appendix B.

After beamforming and matched filtering, the received pressure data are charted onto geographic space using the known source and receiver locations[2,23,24] to generate wide-area sonar images. Examples of images showing targets in NJ2001 and NJ2003 are shown in Figs. 3(A) and 3(B), where the axes show the distance from the moored source and the color scale corresponds to the received normalized scattered pressure levels. In Figs. 3(A) and 3(B), which correspond to a single transmission for the frequency band centered at 415 Hz, the targets are observed to stand 10–25 dB above the background reverberation.

The target-scattered levels are measured for two tracks on May 1, 2001, during the NJ2001 (Tracks 14 and 17), two tracks on May 9, 2003, during NJ2003 (Tracks 201 and 202) and one track on Oct. 2, 2006, during GOM2006 experiment. These tracks, from each of the three experiments, are the ones in which the targets were most clearly observed in wide-area sonar images. It is also observed that the scattered returns fluctuate considerably from one transmission to the next within each track. The mean target-scattered return for a particular track is computed as

$$\tilde{\mathcal{L}}_{\mathrm{meas}} = 10\log_{10}\left(\frac{\sum_{j=1}^{N} \mathrm{MF}(\mathbf{r_j}|\mathbf{r}_0, t_M)}{N}\right), \tag{11}$$

where N is the number of transmissions in the track. The log of measured target-scattered returns normalized by $\tilde{\mathcal{L}}_{\mathrm{meas}}$ [i.e., $10\log_{10}(\mathrm{MF}(\mathbf{r_j}|\mathbf{r_0}, t_M)) - \tilde{\mathcal{L}}_{\mathrm{meas}}$] for all the three experiments are shown as black triangles in Figs. 7–9, respectively. The fluctuation in measured target-scattered return is expected because the experiments were conducted in highly fluctuating waveguides where the acoustic field fluctuates according to complex circular Gaussian random (CCGR) statistics[25–28] due

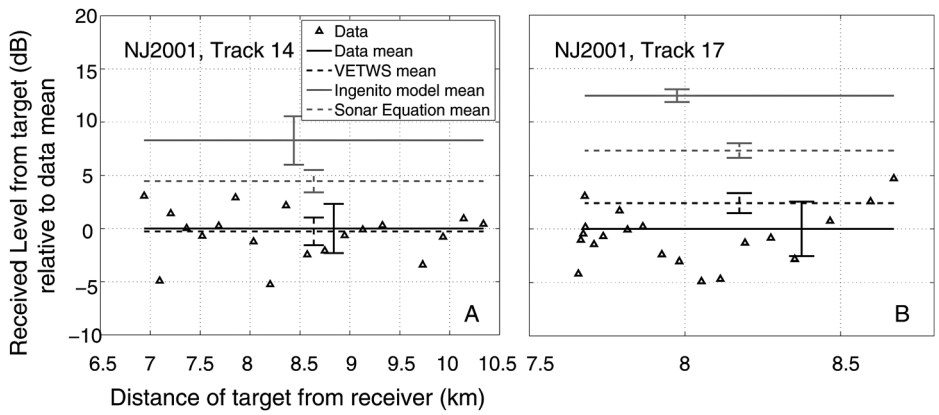

FIG. 7. Comparison of man-made target-scattered levels modeled using the VETWS, Ingenito, and Sonar Equation models relative to the mean scattered level measured during (A) Track 14 of NJ2001 and (B) Track 17 of NJ2001. The center frequency of the source is 415 Hz. Black triangles show the measured target-scattered levels for 19 transmissions made during Track 14 and 20 transmissions made during Track 17, relative to the mean measured level. The standard deviations (SD) of the data for both tracks are 2.5 dB and are marked with solid black vertical lines. The SD of the simulated scattered levels using different models are computed based on Eqs. (15) and (16), and are (1) VETWS: 1.3 dB (Track 14) and 0.93 dB (Track 17); (2) Ingenito model: 2.26 dB (Track 14) and 0.6 dB (Track 17), and (3) Sonar Equation model: 1 dB (Track 14) and 0.7 dB (Track 17).

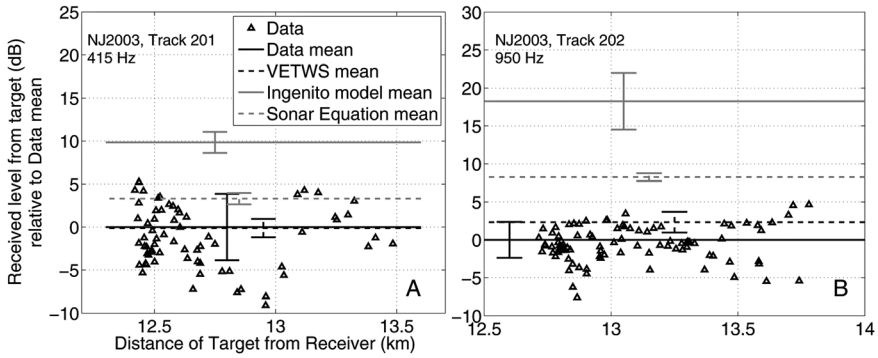

FIG. 8. Comparison of man-made target-scattered levels modeled using the VETWS, Ingenito, and Sonar Equation models relative to the mean scattered level measured during (A) Track 201 and (B) Track 202 of NJ2003. The center frequencies of the source are 415 Hz in Track 201 and 950 Hz in Track 202. Black triangles show the measured target-scattered levels for 89 transmissions made during Track 201 and 90 transmissions during Track 202, normalized to the mean measured scattered level. The SDs of the measurements and the simulated scattered levels using different models are marked with vertical lines and are (1) Data: 3.8 dB (Track 201) and 2.3 dB (Track 202), (2) VETWS: 1 dB (Track 201) and 1.3 dB (Track 202), (3) Ingenito model: 1.2 dB (Track 201) and 3.5 dB (Track 202), and (4) Sonar Equation model: 0.7 dB (Track 201) and 0.5 dB (Track 202).

to the multi-modal or multipath nature of the combined propagation and scattering process. The instantaneous intensity I of a CCGR field follows the exponential distribution, while averaged intensity[25] and the log of averaged intensity[28] follow the gamma and exponential-gamma distributions, respectively, with first and second moments that can be analytically expressed in terms of sample size μ and expected intensity $\langle I \rangle$.[28] The standard deviation of the log of averaged intensity from a CCGR field is given by[28]

$$\sigma = (10 \log_{10} \mathrm{e}) \sqrt{\zeta(2, \mu)} \tag{12}$$

where ζ is the Riemann zeta function. For $\mu = 1$ sample, the standard deviation is 5.6 dB. The number of degrees of freedom μ is expected to increase with the bandwidth of the transmitted signal. For example, for the 50 Hz-bandwidth, 415-Hz center frequency waveforms used in the experiments, μ was experimentally measured to be approximately 1.85 (Ref. 13) and so the standard deviation decreases to approximately 3–4 dB, which is consistent with the experimentally measured standard deviation during the three experiments (Figs. 7–9). To account for the scintillation in measured scattered intensity, the VETWS model is extended to incorporate the waveguide randomness in the next sections and results of numerical simulations are compared to the experimental data.

B. Simulation of target scattered returns using VETWS

In this section, the VETWS model is extended to calculate *broadband* scattered returns from targets in *fluctuating*

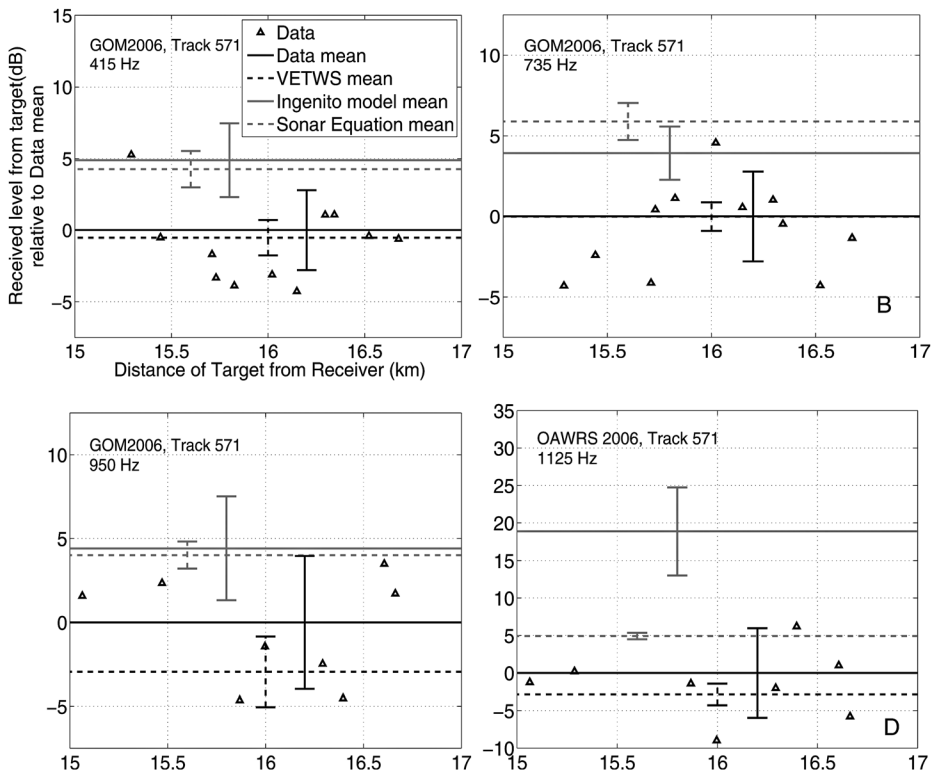

FIG. 9. Comparison of man-made target-scattered levels modeled using the VETWS, Ingenito, and Sonar Equation models relative to the mean scattered level measured during Track 571 of GOM2006 for different source center frequencies (A) 415 Hz, (B) 735 Hz, (C) 950 Hz, and (D) 1125 Hz. Black triangles show the measured target-scattered levels for 10 transmissions when the targets were clearly visible (SNR > 10 dB) during Track 571, normalized to the mean measured scattered level. Fewer transmissions were made per track per frequency during GOM2006 than in NJ2001 and NJ2003. The SDs of the measurements and the simulated scattered levels using different models are marked with vertical lines. For the different frequencies in (A)—(D), the SDs are, respectively, (1) Data: 2.7, 2.7, 3.9, and 5.9 dB; (2) VETWS: 1.2, 0.9, 2, and 1.4 dB; (3) Ingenito model: 2.5, 1.6, 3, and 5.8 dB; and (4) Sonar Equation model: 1.2, 1.1, 0.8, and 0.4 dB.

continental shelf environments. Calculations are made for the different source signals centered at frequencies of 415, 735, 950, and 1125 Hz, which were used in the NJ2001, NJ2003, and GOM2006 experiments.

To compute the received scattered field from Eq. (3), the acoustic field incident on the target, $P_{\text{inc}}(\mathbf{r_t}|\mathbf{r_0}, f)$ and the waveguide Green function from the target to the receiver $G(\mathbf{r}|\mathbf{r_t}, f)$ are calculated using RAM.[16] Note that the coefficients $A_n(z_t|\mathbf{r_0}, f)$ can also be computed using $P_{\text{inc}}(\mathbf{r_t}|\mathbf{r_0}, f)$ as shown in Appendix A. The target-scattered field at the receiver [Eq. (3)] depends on the cylindrical modes of oscillation of the target via A_n, H_n, and H_{n+1}, where n denotes a particular harmonic. For the simulations, it is observed that the solution converges after summing only the first two harmonics ($n = 0, 1$). This is because the targets deployed in all three experiments have a radius that is much smaller than the acoustic wavelength for all the different frequencies used.

Source, receiver, and target center depths used in the model calculations for the different tracks in the three experiments are listed in Table I. For both the New Jersey continental shelf and the Gulf of Maine, a sandy bottom with sound speed of 1700 m/s, density of 1.9 g/cm^3, and attenuation of 0.8 dB/λ (Refs. 9, 14, and 29) is used along with bathymetry and SSPs measured during the experiments. The bottom properties used for acoustic transmission calculations were measured in the same region of the New Jersey continental shelf as the NJ2001 and NJ2003 experiments.[29] These bottom properties have been calibrated with measured bottom reverberation in the New Jersey environment of NJ2001 and NJ2003 (Ref. 14) and with two-way TL in the NJ2001, NJ2003 (Ref. 13), and GOM2006 experiments.[8,9] For each receiver position $\mathbf{r_j}$ along a given track, $M = 20$ Monte Carlo simulations of the target-scattered field are computed. In each simulation, the sound speed profile (SSP) is updated every 500 m (Ref. 30) in range by randomly selecting an SSP from the measured list of profiles, and the acoustic forward propagation[13] is computed. The simulated matched-filtered output for each realization, n, and for each receiver location $\mathbf{r_j}$ is

$$\mathrm{SMF}^{(n)}(\mathbf{r_j}|\mathbf{r}_0, t_M) = \max_t \left| \int P^{(n)}_{\text{scat}}(\mathbf{r_j}|\mathbf{r}_0, f) K Q^*(f) \mathrm{e}^{-i2\pi f(t-t_M)}\, \mathrm{d}f \right|^2. \quad (13)$$

The average simulated matched-filter output for every receiver location $\mathbf{r_j}$ along a track is then computed as

$$\overline{\mathrm{SMF}(\mathbf{r_j})} = \frac{\sum_{n=1}^{M} \mathrm{SMF}^{(n)}(\mathbf{r_j}|\mathbf{r}_0, t = t_M)}{M}. \quad (14)$$

The log of the mean simulated target-scattered return over an entire track is then computed by

TABLE I. Parameters used for modeling target scattering.

	NJ2001	NJ2003	GOM2006
Source depth (m)	32	32	60
Receiver depth (m)	30	30	105
Target center depth (m)	44	44	140

$$\tilde{\mathcal{L}}_{\text{VETWS}} = 10 \log_{10} \left(\frac{\sum_{j=1}^{N} \overline{\mathrm{SMF}(\mathbf{r_j})}}{N} \right) \quad (15)$$

and the standard deviation is given by,

$$\sigma(\overline{\mathrm{SMF}(\mathbf{r_j})}) = \sqrt{\frac{1}{N} \sum_{j=1}^{N} \left(10 \log_{10} \overline{\mathrm{SMF}(\mathbf{r_j})} - \tilde{\mathcal{L}}_{\text{VETWS}} \right)^2} \quad (16)$$

where N is the number of transmissions per track. All average quantities are computed in the intensity domain because a log-transformation introduces an inherent bias to each sample[28] that cannot be removed by averaging the log-transformed samples of the random variable. As in the case of the measured target-scattered returns, the randomization of the ocean waveguide and the use of broadband signals is expected to lead to an expected standard deviation of 3–4 dB for $\mathrm{SMF}^{(n)}(\mathbf{r_j}|\mathbf{r_0}, t_M)$.[31] Averaging over 20 Monte Carlo simulations is then expected to further reduce the standard deviation of $\overline{\mathrm{SMF}(\mathbf{r_j})}$ by $1/\sqrt{20}$, to $\approx$1 dB. This is consistent with numerical simulations of the VETWS-based target scattered returns in all three experiments (Figs. 7–9).

For all simulations of the target-scattered field, it was assumed that the air-filled cylindrical targets used during each field experiment remained vertical in the water column. However, this may not be the case as underwater currents may cause a target to tilt. In Appendix C, it is shown that the effect of target tilt on the received target-scattered levels is not significant because only weak underwater currents prevail in the shallow continental shelf environments where the three experiments were conducted.

C. Simulation of target scattered returns using the Sonar Equation and Ingenito scattering models

In this section, the methodologies used for computing target-scattered returns with both the Ingenito scattering model and the Sonar Equation model are presented. To implement Eq. (4), the mode amplitudes are computed using Eqs. (2A)—(2D) in Ref. 18. The mode functions are computed using the KRAKEN normal mode model[32] and the angle-dependent scatter-function for a pressure-release cylinder is given by[33]

$$S(\alpha, \beta; \alpha_i, \beta_i) = -\frac{kL}{\pi} \mathrm{sinc}\left[\frac{kL}{2} (\cos\alpha_i - \cos\alpha) \right] \times \sum_{m=0}^{\infty} B_m (-j)^m \cos(m[\beta - \beta_i]). \quad (17)$$

The sinc function in the above formula shows that the cylinder scatters like an array in the vertical, while in azimuth it scatters through cylindrical harmonics with amplitudes given by

$$B_m = -\epsilon_m j^m \frac{J_m(ka)}{H_m(ka)}. \quad (18)$$

In Eqs. (17) and (18), α and β are the elevation and azimuth angles of the scattered plane waves, α_i and β_i are the elevation and azimuth angles of the incident plane wave, ϵ_m is the Neumann number defined as $\epsilon_0 = 1$, and $\epsilon_m = 2$ for $m \neq 0$, and J_m is the Bessel function of first kind and order m.

The scattered intensity is computed following Eq. (10) by taking the normalized peak of the matched-filtered broadband scattered field simulated using the Ingenito formulation in Eq. (4). For every receiver location **r,** 20 Monte Carlo simulations of the scattered intensity are performed. For each simulation, one range-independent sound speed profile from the measured profiles during each experiment is picked. The average bathymetry along the source-target-receiver propagation paths is used. The single-frequency scattered field computed using the Ingenito model is expected to follow CCGR statistics because it involves multipath acoustic propagation where scattering and propagation are combined in a double sum over the acoustic modes. Consequently, a 5.6 dB standard deviation is expected for the scattered returns for a single frequency signal. However, the use of multi-frequency signals along with Monte Carlo averaging is expected to lead to smaller standard deviations of 3-4 dB,[13,28] as is seen from Figs. 7–9.

The target-scattered level, according to a depth-averaged sonar equation model is given by

$$RL_{sonar} = SL - TTL + TS_{tgt} \tag{19}$$

where SL is the source-level, TTL is the two-way transmission loss computed for a range- dependent environment and averaged over the target depth, and TS is the target strength of the man-made target in the back-scatter direction, given by

$$TS_{tgt} = 10\log_{10}\left|\frac{S(0,\pi;0,0)}{k}\right|^2. \tag{20}$$

The transmission loss and target strengths are computed for the center frequencies of the different source waveforms used in the field experiments. As in the case of simulations using the VETWS model, for every receiver location, **r,** $M = 20$ Monte Carlo simulations of RL_{sonar} are computed with the sound speed profile being randomized every 500 m in every simulation. The SSPs are randomly selected from the list of measured profiles during each experiment. The target-scattered returns computed using the sonar equation model without any depth averaging of the transmission loss are expected to have a standard deviation of $\sim 5.6\sqrt{2}$ dB, since each single-frequency one-way transmission is expected to have a standard deviation of 5.6 dB[27,28] and forward and back propagation paths factor to a product of two CCGR variables. The averaging of the transmission loss over the target depth and the averaging over 20 Monte Carlo realizations are expected to reduce the standard deviation of RL_{sonar} from its theoretical expected value of $5.6\sqrt{2}$ dB as is indeed found in simulations in Figs. 7–9.

D. Numerical modeling and experimental data comparisons

In this section, results from numerical simulations using the VETWS model, the Sonar Equation model, and the Ingenito scattering model are compared with measured scattered returns from the air-filled cylindrical targets deployed during NJ2001, NJ2003, and the GOM2006 experiments.

The plots in Figs. 7(A) and 7(B) show the log of the measured target scattered returns normalized by $\tilde{\mathcal{L}}_{\text{meas}}$, for two distinct tracks (Tracks 14 and 17) on May 1, 2001, during the NJ2001 experiment. The log of the mean target-scattered returns computed using the three scattering models, normalized by $\tilde{\mathcal{L}}_{\text{meas}}$, are also shown in Fig. 7. The VETWS-mean matches the data-mean to within 0.5 dB for Track 14 and to within 2 dB for Track 17. For both these tracks, the sonar equation model and the Ingenito scattering model overestimate the data mean by approximately 5 and 10 dB, respectively.

A similar comparison is made in Fig. 8 for two tracks on May 9, 2003, during the NJ2003 experiment, corresponding to two source waveforms centered at 415 and 950 Hz. The results are similar to the comparison in Fig. 7. The VETWS-mean matches the data mean to within 0.1 dB for the 415 Hz centered source signal and to within 2 dB for the 950-Hz centered source signal. Again both the sonar equation model and the Ingenito scattering model overestimate mean scattered levels by more than 5 dB.

During the GOM2006 experiment, four 50-Hz bandwidth LFM waveforms with center frequencies 415, 735, 950, and 1125 Hz were transmitted during each track. The long inter-transmission time (75 s) and inter-leaving of frequencies leads to fewer data points available per waveform per track than in the NJ2001 and NJ2003 experiments. Figure 9 shows the log of the measured target scattered returns, with $\tilde{\mathcal{L}}_{\text{meas}}$ subtracted, for Track 571 on Oct. 2, 2006, during the GOM2006 experiment, for all four waveforms transmitted. The VETWS-mean matches the data-mean to within 0.5 dB for the 415 - and 735-Hz centered source signals and to within 3 dB for the 950 - and 1125-Hz centered source signals. The sonar equation model and the Ingenito scattering model overestimate the data by more than 4 dB.

VI. CONCLUSION

Bistatic, long-range measurements of acoustic scattered returns from vertically extended, air-filled tubular targets were made during three distinct field experiments in fluctuating continental shelf environments. It is shown that Sonar Equation estimates of mean target-scattered intensity lead to large errors, differing by an order of magnitude from both the measurements and waveguide scattering theory. This is because the sonar equation approximation is not generally valid for targets with directional scatter functions in an ocean waveguide. The use of the Ingenito scattering model is also shown to lead to significant errors in estimating mean target-scattered intensity in the field experiments because they were conducted in range-dependent ocean environments with large variations in sound speed structure over the depth of the targets, scenarios that violate basic assumptions of the Ingenito model. Green's theorem based full-field modeling (VETWS) that describes scattering from vertically extended cylindrical targets in range-dependent ocean waveguides by

taking into account nonuniform sound speed structure over the target's depth extent is shown to accurately describe the statistics of the targets scattered field in all three field experiments, for example, yielding mean intensity level estimates within the 3 dB standard deviation of the data. To account for the scintillation in the measured scattered intensity caused by fluctuations of the ocean waveguide, Monte Carlo simulations of the scattered field are computed by implementing the full-field model in a range-dependent environment randomized by internal waves. Returns from the man-made target are also shown to have a very different spectral dependence from the dominant fish clutter measured in each experiment, suggesting that multi-frequency measurements may often be used to help distinguish fish from man-made targets.

ACKNOWLEDGMENTS

This research was supported by the U.S. Office of Naval Research, the Alfred P. Sloan Foundation, the U.S. National Oceanographic Partnership Program, and is a contribution to the Census of Marine Life.

APPENDIX A: ALTERNATE METHOD FOR COMPUTING COEFFICIENTS A_n

In Ref. 10, the coefficients $A_n(z_t|\mathbf{r_0}, f)$ were estimated using a least squares approach. Here, we obtain exact analytic expressions for the coefficients by exploiting the orthogonality property of the cylindrical modes. From Eq. (3) in Ref. 10,

$$P_{\text{scat}}(\rho_t = a, \phi_t, z_t|\mathbf{r}_0,f) = \sum_{n=0}^{\infty} A_n(z_t|\mathbf{r}_0,f)\mathrm{H}_n^{(1)}(ka)\cos(n\phi_t). \tag{A1}$$

For a pressure release target, the total pressure on its surface is zero and so,

$$P_{\text{scat}}(\rho_t = a, \phi_t, z_t|\mathbf{r}_0,f) = -P_{\text{inc}}(\rho_t = a, \phi_t, z_t|\mathbf{r}_0,f). \tag{A2}$$

Multiplying both sides by $\cos(m\phi_t)$ and integrating over ϕ_t,

$$\int_{\phi_t=0}^{2\pi} \sum_{n=0}^{\infty} A_n(z_t|\mathbf{r}_0,f)\mathrm{H}_n^{(1)}(ka)\cos(n\phi_t)\cos(m\phi_t)d\phi_t = -\int_{\phi_t=0}^{2\pi} P_{\text{inc}}(a, \phi_t, z_t|\mathbf{r}_0,f)\cos(m\phi_t)d\phi_t. \tag{A3}$$

But,

$$\int_{\phi_t=0}^{2\pi} \cos(n\phi_t)\cos(m\phi_t)\,\mathrm{d}\phi_t = \begin{cases} 0, & n \neq m \\ \pi, & n = m \neq 0 \\ 2\pi, & n = m = 0. \end{cases} \tag{A4}$$

Thus,

$$A_m(z_t|\mathbf{r}_0,f) = \begin{cases} \dfrac{-\int_{\phi_t=0}^{2\pi} P_{\text{inc}}(a,\phi_t,z_t|\mathbf{r}_0,f)\cos(m\phi_t)\mathrm{d}\phi_t}{\pi\mathrm{H}_m^{(1)}(ka)}, & m\neq 0 \\ \dfrac{-\int_{\phi_t=0}^{2\pi} P_{\text{inc}}(a,\phi_t,z_t|\mathbf{r}_0,f)\,\mathrm{d}\phi t}{2\pi\mathrm{H}_0^{(1)}(ka)}, & m=0. \end{cases} \tag{A5}$$

APPENDIX B: EFFECT OF OCEANOGRAPHY ON ARRIVAL STRUCTURE OF TARGET SCATTERED RETURNS

Acoustic returns from targets are either sharp and well localized or dispersed in sonar imagery (Fig. 4). It is shown that changes in oceanography, such as the sound speed structure in the water column can cause dispersion in target returns.

The example of target scattering in the New Jersey continental shelf, shown in Figs. 4(D)–4(I), is considered to simulate the matched filter output for different oceanographic conditions. Figure 10(A) shows the SMF output [Eq. (13)] for one particular measured sound speed profile (SSP) used as input in the simulation, where the target is predicted as a sharp, well-localized return. The Green function used in the

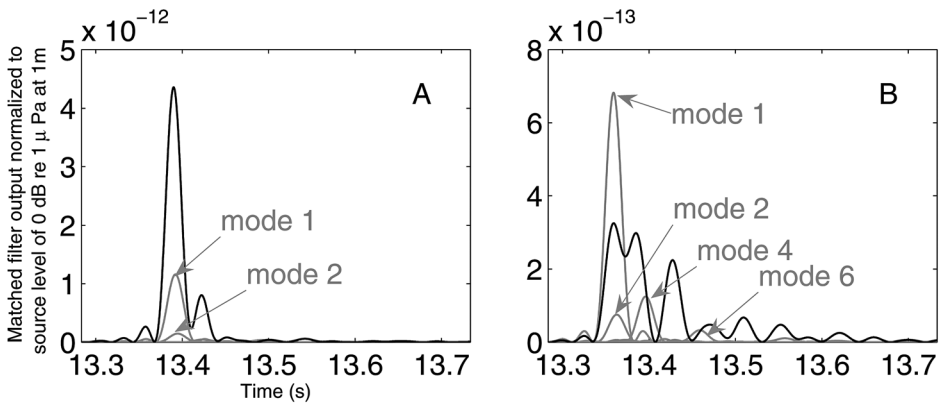

FIG. 10. Square of the base-band envelope of the matched filtered scattered returns from man-made, air-filled cylindrical targets simulated using the VETWS model for different oceanographic conditions in the New Jersey environment. The different dominant acoustic modes are marked in gray. The modes combine either constructively or destructively to form the total scattered return, which is marked in black. (A) Example of sharp, well-localized return from target with most of the scattered energy concentrated in the first two modes. (B) Example of dispersed return from target with scattered energy distributed across more modes than in (A). The same source-receiver-target geometry of (A) was used but with a different sound speed profile.

VETWS model is computed using the KRAKEN normal-mode propagation model. The modal contribution to the total SMF output, also shown in the figure, indicates that most of the energy is concentrated in the first few modes. These first few modes have very similar propagation speeds and so arrive almost at the same time at the receiver, resulting in good localization of the man-made target. This figure is comparable with Fig. 4(E), which shows one measured MF output [Eq. (10)] during Track 201 of the NJ2003 experiment. By using a different SSP, however, the SMF output in Fig. 10(B) shows a dispersed arrival structure with the acoustic energy distributed over more modes than in Fig. 10(A) and is comparable to Fig. 4(H). The significant contributions from higher order modes that arrive later implies that the target appears more weak and more dispersed in sonar imagery. Note that the individual modal amplitudes in Figs. 10(A) and 10(B) are very similar, but they combine differently in both cases.

APPENDIX C: EFFECT OF TARGET TILT ON SCATTERED RETURNS

In the theoretical formulation (Sec. IV B), we have assumed that the air-filled cylindrical targets remain vertical in the water column. During field measurements, however, there is the possibility that the targets may tilt due to the action of underwater currents.

To quantify the effect of target tilt on target scattered field measurements, the VETWS model, strictly developed for vertically extended targets, is modified to include target tilt. The effect of target tilt on the received scattered level is expected to be maximum when the tilt is in the plane defined by the source/receiver, and the vertical through the target center because the target beams like a vertical array [Eq. (17)]. To include target tilt, the coordinate system used in Eq. (3) is tilted such that any point on the target is given by $\bar{\mathbf{r}}_t = (\rho_t, \phi_t, z_t)$, and the source and receiver positions are given by

$$\bar{\mathbf{r}}_{tilted} = (\rho \cos\theta + z \cos\theta, 0, z \cos\theta - \rho \sin\theta), \quad \text{(C1)}$$

$$\bar{\mathbf{r}}_{0,tilted} = (\rho_0 \cos\theta + z_0 \cos\theta, 0, z_0 \cos\theta - \rho_0 \sin\theta), \quad \text{(C2)}$$

where $(\rho_0, 0, z_0)$ and $(\rho, 0, z)$ are the source and receiver positions in the original untilted coordinate system and θ is the tilt angle. The modified VETWS model is used to compute the scattered levels as a function of in-plane tilt by averaging Monte Carlo simulations, following the procedure described in Sec. V B. The approach is also repeated for different source frequencies.

For illustration, the New Jersey environment is used in our modified-VETWS model simulations, with a monostatic source-receiver configuration. Figure 11 shows the expected SMF for 415 and 950 Hz as a function of target tilt angle after averaging over 50 Monte Carlo simulations. We find that the average SMF is most sensitive to tilt at the higher frequency of 950 Hz and least sensitive at 415 Hz. The next step is to quantify the target tilt that we expect in the New Jersey continental shelf.

In the absence of other external biological or man-made disturbances, target-tilt depends on the prevailing underwater currents at the target depth. The tilt, as a function of current speed is calculated by balancing the buoyant force of the air-filled target with the current-induced drag force on the target.

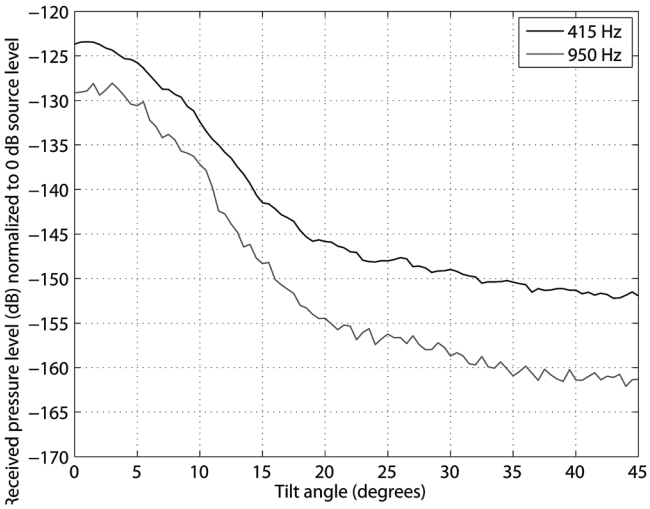

FIG. 11. Effect of target tilt on received pressure levels. Simulations of target-scattered levels, computed using a modified VETWS model described in Sec. VI as a function of target-tilt angle for two different frequencies used during NJ2003. A monostatic source-receiver configuration as described in Sec. VI is used. The target is assumed to tilt in the plane formed by the vertical through the target center and the source location.

In the New Jersey strataform, the strongest currents are found just off the continental shelf, along the shelf break, at water depths $\geq$100 m.[34,35] During the NJ2001 and NJ2003 experiments, the targets were deployed in much shallower waters on the shelf (water depth $\approx$70 m) where current speeds are expected to be low (about 0.1 m/s).[36]

The usual 0.1 -m/s current speeds lead to target tilts of less than 2°, which suggests very small changes in target-scattered levels (Fig. 11). Occasional 0.5-m/s current speeds,[36] however, can result in target tilts of 12°, which suggests a reduction in target-scattered levels of 10 dB (Fig. 11). Such current bursts would then result in a dramatic reduction (tens of decibels) in target scattered levels over a period of several hours, a phenomenon that was not observed during both the NJ2001 and NJ2003 experiments.

In the Gulf of Maine, the deep location of the targets (140–180 m) ensures that current speeds of less than 0.1 m/s prevail at the target depth.[34,35] For such small current speeds, the target tilts and subsequently its effect on target scattered levels are negligible.

[1]C. I. Malme, "Development of a high target strength passive acoustic reflector for low- frequency sonar applications," IEEE J. Ocean. Eng. **19**, 438–448 (1994).
[2]P. Ratilal, Y. Lai, D. Symonds, L. A. Ruhlmann, J. R. Preston, E. K. Scheer, M. T. Garr, C. W. Holland, J. A. Goff, and N. C. Makris, "Long range acoustic imaging of the continental shelf environment: The Acoustic Clutter Reconnaissance Experiment 2001," J. Acoust. Soc. Am. **117**, 1977–1998 (2005).
[3]P. Ratilal, Y. Lai, and N. Makris, "Validity of the sonar equation and babinet's principle for scattering in a stratified medium," J. Acoust. Soc. Am. **112**, 1797–1816 (2002).
[4]R. J. Urick, *Principles of Underwater Sound* (Mc-Graw Hill, New York, 1983), pp. 17–30.
[5]F. Ingenito, "Scattering from an object in a stratified medium," J. Acoust. Soc. Am. **82**, 2051–2059 (1987).

[6]N. C. Makris, P. Ratilal, D. T. Symonds, S. Jagannathan, S. Lee, and R. Nero, "Fish population and behavior revealed by instantaneous continental-shelf-scale imaging," Science **311**, 660–663 (2006).
[7]S. Jagannathan, I. Bertsatos, D. T. Symonds, T. Chen, H. T. Nia, A. Jain, M. Andrews, Z. Gong, R. Nero, L. Ngor, M. Jech, O. R. Godø, S. Lee, P. Ratilal, and N. C. Makris, "Ocean acoustics waveguide remote sensing (OAWRS) of marine ecosystems," Mar. Ecol. Prog. Ser. **395**, 137–160 (2009).
[8]N. C. Makris, P. Ratilal, S. Jagannathan, Z. Gong, M. Andrews, I. Bertsatos, O. Godoe, R. Nero, and M. Jech, "Critical population density triggers rapid formation of vast oceanic fish shoals," Science **323**, 1734–1737 (2009).
[9]Z. Gong, M. Andrews, S. Jagannathan, R. Patel, J. M. Jech, N. C. Makris, and P. Ratilal, "Low-frequency target strength and abundance of shoaling atlantic herring clupea harengus in the gulf of maine during the ocean acoustic waveguide remote sensing (OAWRS) 2006 experiment," J. Acoust. Soc. Am. **127**, 104–123 (2010).
[10]E. T. Küsel and P. Ratilal, "Effects of incident field refraction on scattered field from vertically extended cylindrical targets in range-dependent ocean waveguides," J. Acoust. Soc. Am. **125**, 1930–1936 (2009).
[11]G. L. Turin, "An introduction to matched filters," IRE Trans. Inf. Theory **IF6**, 311–329 (1960).
[12]N. Levanon, *Radar Principles* (Wiley, New York, 1988), pp. 101–120.
[13]M. Andrews, T. Chen, and P. Ratilal, "Empirical dependence of acoustic transmission scintillation statistics on bandwidth, frequency, and range on New Jersey continental shelf," J. Acoust. Soc. Am. **125**, 111–124 (2009).
[14]A. Galinde, N. Donabed, M. Andrews, S. Lee, N. C. Makris, and P. Ratilal, "Range-dependent waveguide scattering model calibrated for bottom reverberation in a continental shelf environments," J. Acoust. Soc. Am. **123**, 1270–1281 (2008).
[15]M. Andrews, Z. Gong, and P. Ratilal, "Effects of multiple scattering, attenuation and dispersion in waveguide sensing of fish," J. Acoust. Soc. Am. **130**, 1253–1271 (2011).
[16]M. D. Collins, "A split-step Padé solution for the parabolic equation method," J. Acoust. Soc. Am. **93**, 1736–1742 (1993).
[17]N. C. Makris and P. Ratilal, "OAWRS Gulf of Maine 2006 Experiment Cruise Report," Technical Report, MIT and NU MA (2006).
[18]N. C. Makris and P. Ratilal, "A unified model for reverberation and submerged object scattering in a stratified ocean waveguide," J. Acoust. Soc. Am. **109**, 909–941 (2001).
[19]N. C. Makris, "A spectral approach to 3-D object scattering in layered media applied to scattering from submerged spheres," J. Acoust. Soc. Am. **104**, 2105–2113 (1998).
[20]R. H. Hackmann and G. S. Sammelmann, "Multiple scattering analysis for a target in an ocean waveguide," J. Acoust. Soc. Am. **84**, 1813–1825 (1988).
[21]P. Ratilal and N. C. Makris, "Mean and covariance of the forward field propagated through a stratified ocean waveguide with three-dimensional random inhomogeneities," J. Acoust. Soc. Am. **118**, 3532–3559 (2005).
[22]J. J. Bowman, T. B. A. Senior, and P. L. E. Uslenghi, *Electromagnetic and Acoustic Scattering by Simple Shapes* (Hemisphere Publishing, New York, 1987), pp. 1–20.
[23]N. C. Makris and J. M. Berkson, "Long-range backscatter from the Mid-Atlantic Ridge," J. Acoust. Soc. Am. **95**, 1865–1881 (1994).
[24]N. C. Makris, L. Z. Avelino, and R. Menis, "Deterministic reverberation from ocean ridges," J. Acoust. Soc. Am. **97**, 3547–3574 (1995).
[25]J. W. Goodman, *Statistical Optics* (Wiley, New York, 1985), p. 108.
[26]G. Bergmann, "Intensity fluctuations," in *The Physics of Sound in the Sea, Part 1: Transmission* (National Defense Research Committee, Washington, DC, 1948), pp. 158–173.
[27]I. Dyer, "Statistics of sound propagation in the ocean," J. Acoust. Soc. Am. **48**, 337–345 (1970).
[28]N. C. Makris, "The effect of saturated transmission scintillation on ocean acoustic intensity measurements," J. Acoust. Soc. Am. **100**, 769–783 (1996).
[29]J. A. Goff, B. J. Kraft, L. A. Mayer, S. G. Schock, C. K. Sommerfield, H. C. Olson, S. P. S. Gulick, and S. Nordfjord, "Seabed characterization on the New Jersey middle and outer shelf: correlatability and spatial variability of seafloor sediment properties," Mar. Geol. **209**, 147–172 (2004).
[30]T. Chen, P. Ratilal, and N. C. Makris, "Mean and variance of the forward field propagated through three-dimensional random internal waves in a continental-shelf waveguide," J. Acoust. Soc. Am. **118**, 3560–3574 (2005).
[31]M. Andrews, Z. Gong, and P. Ratilal, "High-resolution population density imaging of random scatterers through cross-spectral coherence in matched filter variance," J. Acoust. Soc. Am. **126**, 1057–1068 (2009).
[32]M. B. Porter, "The Kraken normal mode program, user's manual," Technical Report, SACLANT Undersea Research Centre, La Spezia, Italy (1991).
[33]H. C. van de Hulst, *Light Scattering by Small Particles* (Dover, New York, 1956), pp. 297–322.
[34]J. S. Allen, R. C. Beardsley, J. O. Blanton, W. C. Boicort, B. Butman, L. K. Coachman, T. H. K. A. Huyer, T. C. Royer, J. D. Schumacher, R. L. Smith, W. Sturges, and C. D. Winant, "Physical oceanography of continental shelves," Rev. Geophys. Space Phys. **21**, 1149–1181 (1983).
[35]G. T. Csanady, "On the theories that underlie our understanding of continental shelf circulation," J. Oceanogr. **53**, 207–229 (1997).
[36]Z. R. Hallock and R. L. Field, "Internal-wave energy fluxes on the New Jersey shelf," J. Phys. Oceanogr. **35**, 3–12 (2005).